

Temporal Evolution of flow in Pore-Networks: From Homogenization to Instability

Ahmad Zareei,* Deng Pan,* and Ariel Amir†

School of Engineering and Applied Sciences, Harvard University, Cambridge, MA, 02148

(Dated: May 20, 2021)

We study the dynamics of flow-networks in porous media using a pore-network model. First, we consider a class of erosion dynamics assuming a constitutive law depending on flow rate, local velocities, or shear stress at the walls. We show that depending on the erosion law, the flow may become uniform and homogenize, stay as it is, or become unstable and develop channels. By defining an order parameter capturing different behaviors we show that a phase transition occurs depending on the erosion dynamics. Using a simple model, we identify quantitative criteria to distinguish these regimes that correctly predicts the fate of the network given at erosion or at early stages of clogging.

Rephrased
definitions
including

Fluid flow through a porous medium undergoing a dynamical change in its network of micro-structure is a challenging problem and has many environmental and industrial applications^{1–14}. The disordered pore structure of a porous medium results in heterogeneously distributed fluid flow between the pores. Due to the fluid flow, the pore structure can further change dynamically either through the erosion of pore boundary walls or deposition/sedimentation of material on the boundary of the pores. Such heterogeneous and dynamical changes of the solid structure affect the pore-level fluid flow which in turn affects the dynamical changes to the pore structure. This feedback mechanism along with the initial heterogeneous fluid flow complicates the dynamical process and makes it difficult to understand and predict the porous media behavior. Nonetheless, an understanding of the dynamical change is essential to improve any of the porous media applications where the pore network changes over time, applications such as groundwater remediation and precipitation of minerals in rocks¹⁵, biofilm growth in water filtration, and protective filters^{4–8}, as well as enhanced oil recovery with polymer flooding^{16,17}, or water-driven erosion^{18,19}.

In order to model erosion in porous materials, different models have been used where erosion is assumed to be locally proportional to different flow parameters, such as shear stress at the walls^{20–23}, or power dissipation by flow^{24–26}. Recently, it has been shown that using a coarse-grained model with an erosion rate depending on the local pressure gradient, branching instability can be reached where its topology is determined by the geometry of external flow forcing^{19,27}. Similar to erosion, in clogging, various deposition rates^{28–30} have been used either depending on local fluid flux, velocity, or at a constant rate independent of any flow parameters. In order to unify different approaches, we use a general constitutive model which embeds different erosion or clogging dynamics and as a result allows us to study the effect of different dynamics conjointly. Additionally, we use a network approach^{31–35} to study the flow dynamics in the porous media, since it has the advantage of capturing flow statistics without requiring a coarse-grained homogenization and is computationally efficient which allows

for larger domain simulations.

The network of pores inside the solid structure is connected together through pore-throats that effectively show resistance to the fluid flow between the pores (Fig. 1a). Network-based models have been successfully shown to capture key properties of fluid flow in a porous material such as the probability distribution of fluid flux³¹, the permeability scaling during clogging³⁶, or the first fluidized path in a porous structure³⁷. The degradation of the solid skeleton (i.e., erosion) or deposition of material on the pore throats (i.e., clogging) in such networks is modeled by the change (increase or decrease) in the radius of the edges connecting the pores which translates into changes in the flow resistance between the pores. Using a general local erosion law that can model different dynamics, we show a variety of behaviors are possible. Using numerical simulations we show the emergence of two behaviors and morphologies (i.e., channelization instability or homogenization) are possible through selective erosion and subsequent flow enhancement. We develop a simplified model to capture the underlying physics and furthermore show a phase transition occurs depending on the parameters of the model.

Methods and Results— We consider low-Reynolds fluid flow through the porous network, i.e., $\rho u / \mu \ll 1$ where ρ is the fluid density and μ is the kinematic viscosity, u and r are characteristic fluid velocity and pore radius. In such conditions, the fluid flow in each tube follows the Poiseuille law $p_i - p_j = (8\mu l_{ij}/\pi r_{ij}^4)q_{ij}$ where p_i, p_j represent pressures at neighboring nodes i, j , and r_{ij}, l_{ij}, q_{ij} are respectively the radius, length, and fluid flow rate at the edge connecting pores i and j . The coefficient $\pi r_{ij}^4/8\mu l_{ij}$ which relates the fluid flux to the pressure difference can be considered as the conductance C_{ij} of the edge ij in the pore-network. Solving for the conservation of the mass at all pores (inset in Fig. 1b), the pressure distribution over the nodes can be obtained (see supplementary material section S1). Initially, we consider a topologically random network of nodes constructed using a uniform distribution of $N_x \times N_y$ nodes in a planar domain where the nodes' connectivity are obtained using Delaunay triangulation (see Fig. 1b(i) for

I don't think
this is the
right word...

New paragraph.

② Redundant!

Say it
in
titles
network!

Redundant
with
later
parts.

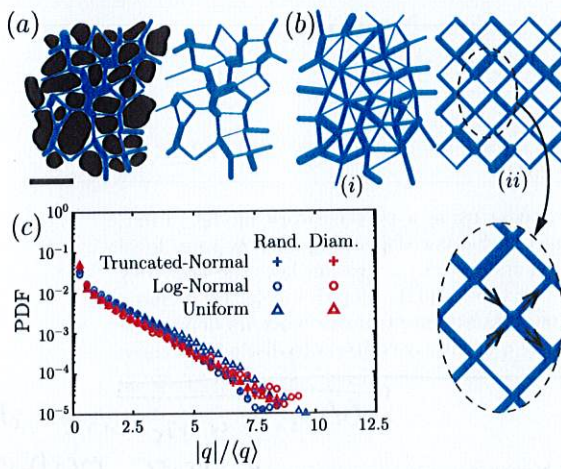


FIG. 1. (a) Cross section of a porous sandstone sample obtained using computerized tomography³⁸. The scale in the bottom left shows 1mm. The network of pores and throats is highlighted in blue. In the network model, the pores are represented with nodes and the throats between pores are approximated with tubes connecting the pores together. (b) Schematic of a topologically random network (i); and a structured diamond grid network (ii). The edge diameters in both networks are randomly distributed. The inset figure shows the conservation of mass at each node. (c) The universal probability distribution function (PDF) of fluid flux for a topologically random (in blue) or diamond network (red) with a highly disordered random net including uniform (triangles), log-normal (circles), and truncated normal (plus) distributions.

a part of such network). The radius of the edges is considered as independent and identically distributed random variables sampled from a probability distribution that can be either uniform, log-normal, or a truncated normal distribution (see supplementary material S1 for more details). Assuming a pressure difference between the boundary nodes at the left and the right boundary, the pressure at the nodes and the fluid flow rate at the tubes can be obtained by solving the corresponding set of linear equations. We find that for large enough randomness in the edge radii (i.e., $\text{std}(r_{ij})/\text{mean}(r_{ij}) \geq 0.5$), the PDF is well described by a single exponential distribution as shown in Fig. 1c. The exponential form of the PDF reflects the relatively small number of edges with extremely large fluid fluxes. The exponential distribution of fluid flux obtained here is similar to earlier experimental and numerical measurements^{31,36,39}. Considering a structured diamond-grid of pores (Fig. 1b(ii)) which significantly simplifies the geometrical complexity of the network, we find that the PDF of normalized fluid flux remains unchanged for various distributions 1c). The diamond grid allows one to calculate the mean-field approximation of fluid flux distribution (see supplementary material S2) using similar idea proposed for the force distribution in granular materials^{31,40,41}. Particularly, it can be shown that the PDF of normalized fluid flux

inside a highly disordered porous material converges to a universal distribution with an exponential form, i.e., $p(\hat{q}) \propto e^{-\alpha\hat{q}}$ for large \hat{q} where \hat{q} is the normalized fluid flux $\hat{q} = q/\langle q \rangle$ (see supplementary materials S2). This result indicates a simple method to capture the statistics of heterogeneous fluid flow inside a topologically ordered porous material.

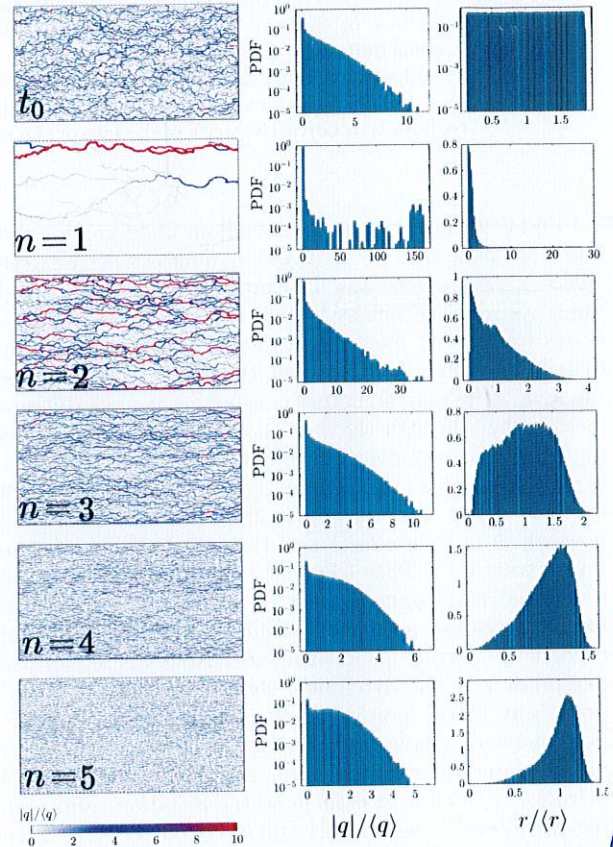


FIG. 2. Erosion in a network of pipes. The initial condition is shown with the label $t = 0$ in the first row. Each row afterward corresponds to the simulation result at $t = T$ where $\langle r_{t=T} \rangle = 2r_0$ with $r_0 = \langle r_{t=0} \rangle$. The erosion law is based on Eq. (1) where $m = 1$ and different powers of n correspond to different models of erosion. The first, second, and third columns are snapshots of the pore network, the PDF of normalized fluid flux $q/\langle q \rangle$, and the PDF of normalized radius $r/\langle r \rangle$ at $t = T$ respectively.

In order to model erosion in porous media, we consider the abrasion in the throats which correspond to the change in the radius of the edges in the network. We model the dynamics of the change in the radius as

$$\frac{dr_{ij}}{dt} = \alpha \frac{|q_{ij}|^m}{r_{ij}^n}, \quad (1)$$

where m, n, α are constants. Different powers of m and n along with a positive $\alpha > 0$ correspond to different

erosion physics. Particularly, the erosion when $m = 1$ and (i) $n = 0$ depends on the amount of flux q_{ij} passing through the edge; (ii) $n = 2$ depends on the local velocities; (iii) $n = 3$ depends on the shear force at the boundary of the throat. Additionally, $m = 2$ and $n = 6$ corresponds to the models considered in biological transport networks where the radius changes proportional to the square of shear stress at the boundary walls^{42,43}. We consider a randomly initialized network with highly disordered diameters obtained from a uniform distribution (see supplementary material S1). The flow inside the pores, PDF of flux in the tubes, and PDF of tube radii are shown in Fig. 2. We assume a constant pressure difference between the left and the right boundaries. In each time step, we increase the local radius of the tubes based on the erosion law introduced in Eq. (1). Since different physics of erosion requires linear dependence of erosion to the flow parameters (such as fluid flux, velocity, or shear stress at the walls), we chose $m = 1$. Later we will address the network's behavior for different powers of m .

We continue the simulations until $\langle r \rangle = 2r_0$. The results of the simulations for different n are shown in Fig. 2. When $n = 1$ or 2, the network develops channels. In such cases, the flow is dominated by a few edges carrying most of the flow while the rest of the network carries almost no flow. This can be seen in the PDF of the normalized radius which becomes bimodal. Furthermore, the PDF of the normalized fluid flux contains a small number of edges with very large flux values while the majority of the edges carry small flux. Contrary to $n = 1, 2$, when $n = 3$ and the erosion depends on shear at the throats' boundary walls, we find that the flow patterns stay very close to the initial shape, however, with larger and exacerbated flux values. Although the maximum fluid flux increases, the PDF of normalized fluid fluxes remains almost exponential, and the PDF of diameters moves toward larger values. Increasing n to larger values, $n = 4$ or 5, we find that the flow pattern in the network moves toward homogenization. Here, the tail of the normalized fluid flux distribution retracts and the distribution moves toward the average value. We further find that the PDF of the diameters moves toward the average and the coefficient of variation reduces. It is to be noted that a similar result upholds in a 3d random network of tubes or 2d topologically ordered (diamond grid) network of tubes with wide random distribution of diameters, as well as 2d random network with a narrow distribution of diameters (see supplementary material S3). These results suggest that the the observed network behavior is robust with respect to the network topology or randomness in the diameters of network's tubes.

disorder *strength*.

Simplified Model— In order to understand the underlying reason behind the transition in network behavior during erosion for different powers of n , we focus on a simplified model with only two tubes in parallel or series (see Fig. 3a,b). First, assuming two cylindrical tubes with radii r_1, r_2 in series and connected back to back, the flow is the same for the two tubes $q_1 = q_2 = q$ (Fig. 3a). The

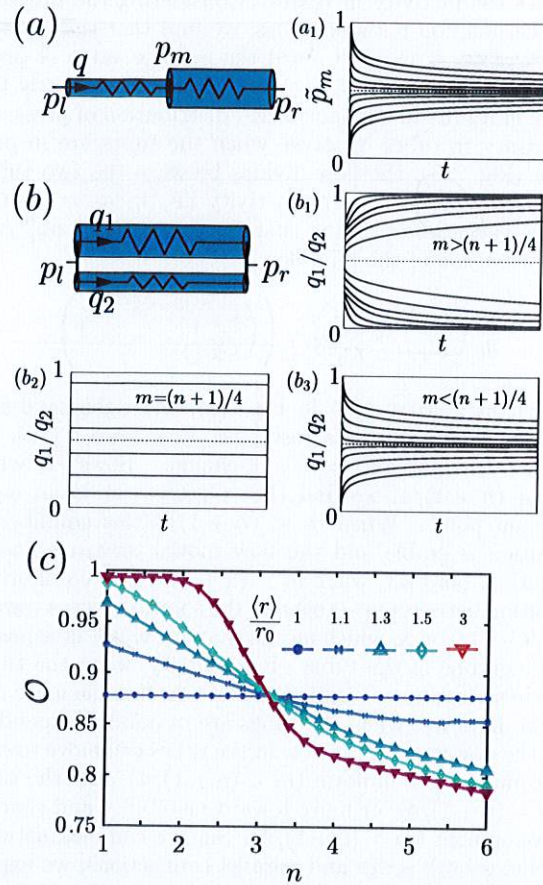


FIG. 3. Two tubes in (a) series or (b) parallel configuration. The tube radius dynamically change with the erosion law (Eq. (1)). When the tubes are in series, we find that for any m, n , (a₂) the normalized pressure at the middle junction between the tubes $\tilde{p}_m = (p_m - p_l)/(p_r - p_l)$ approaches $1/2$ which results in a homogenized pressure distribution. When the tubes are in parallel, initially the flow is distributed among the tubes proportional to their flow conductivity C_1, C_2 . After erosion, we find that (b₁) when $m > (n+1)/4$, the entire flow eventually passes through one of the tubes, and channeling occurs; (b₂) when $n = 3$, the flow ratio between the pipes does not change over time; and (b₃) when $m < (n+1)/4$ the flow distributes between the tubes equally and $q_1/q_2 \rightarrow 1$ which results in the homogenization of the network. (c) Order parameter \mathcal{O} calculated from simulation results presented in Fig. 2 for different powers of n with $m = 1$ plotted over time as the network structure is eroded. In a random network, when $n < 3$ the order parameter increases ($\mathcal{O} \rightarrow 1$) while the network is developing channels, and when $n > 3$ the order parameter decreases ($\mathcal{O} \rightarrow 0$) while the network moves toward homogenization, and when $n \approx 3$ the order parameter stays constant while the network statistics remains unchanged.

radius of each tube then changes with $dr_i/dt = \alpha q^m / r_i^n$ where $i = 1, 2$. As a result, we find that the conductivity of each tube changes as $dC_i/dt \propto q^m C_i^{(3-n)/4}$, where each

tube's conductivity increases. Considering the pressure at the junction between tubes, we find that ~~this middle point pressure~~ moves toward the average value of pressure on both sides (see Fig. 3(a₁)) and consequently the erosion results in a homogenized distribution of pressure. Contrary to tubes in series, when the tubes are in parallel (Fig. 3b), the flow divides between the two tubes proportional to their conductivity in $q_1/q_2 = C_1/C_2$. Since each tube's radius changes as $dr_i/dt = \alpha q_i^m/r_i^n$, the evolution of the fluid flow ratio becomes

$$\frac{d}{dt} \left(\frac{C_1}{C_2} \right) \propto \frac{C_1}{C_2^{n/4+1}} \left(\left(\frac{C_1}{C_2} \right)^{m-\frac{n+1}{4}} - 1 \right). \quad (2)$$

When $m = (n+1)/4$ in Eq. (2), the right-hand-side becomes zero and as a result the flow ratio C_1/C_2 remains constant and does not change. However, when $m \neq (n+1)/4$, we find that $C_1/C_2 = 1$ is an equilibrium point. When $m < (n+1)/4$ this equilibrium solution is stable and the flow moves toward homogenization; however, when $m > (n+1)/4$ this equilibrium solution becomes unstable and the solution moves toward $C_1/C_2 \rightarrow 0$ or ∞ which means that the ~~whole~~ flow passes through one of the tubes. In summary, when the tubes are in series any erosion law makes flow become more uniform; however, when the tubes are in parallel depending on the powers m, n the flow in the tubes can move toward becoming more uniform ($m < (n+1)/4$), stay the same ($m = (n+1)/4$), or move toward instability and channel development ($m > (n+1)/4$). Since a complex network includes both series and parallel connections, we expect that the whole network structure behaves in a similar manner with a transition in the networks behavior at $n = 3$. This observation ~~here~~ is consistent with the numerical simulation results shown in Fig. 2.

Phase transition—In order to quantify the transition of the network between channeling instability and homogenization, we define an order parameter

$$\mathcal{O} = \frac{1}{N-1} \left(N - \frac{\left(\sum_{ij} q_{ij}^2 \right)^2}{\sum_{ij} q_{ij}^4} \right) \quad (3)$$

where N is the number of edges. The order parameter defined here is inspired by the participation ratio (PR) employed to quantify the localization of an eigenstate in the analysis of Anderson localization⁴⁴. The order parameter $\mathcal{O} = 0$ when the flux in all the edges become the same $q_{ij} = \bar{q}$. On the other hand, when fluid flux becomes highly localized with only a few edges with non-zero flux, $\mathcal{O} \rightarrow 1$. We numerically calculated the average order parameter \mathcal{O} for randomly initialized networks averaged over 20 different realizations. The results are shown in Fig. 3c for different amounts of erosion measured by the increase in the average diameter $\langle r \rangle / r_0$. As shown in Fig. 3c, at $n \approx 3$ the order parameter remains unchanged; however for $n > 3$ the order parameter moves toward zero, where the flow becomes more uniform, and

for $n < 3$ the order parameter goes toward unity, where channels are developed. ~~The transition in the order parameter indicates a phase transition at $n = 3$ in the long-time behavior of the network which is in agreement with the toy model prediction and simulation results in Fig. 2.~~ This

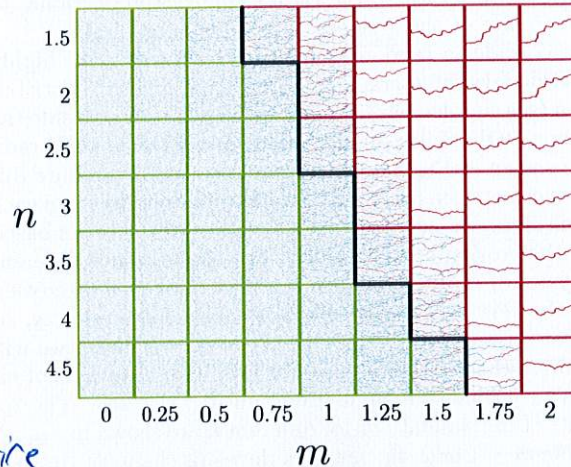


FIG. 4. Evolution of a randomly initialized network for various powers of m and n in Eq. (1). The network is randomly initialized with 50×50 randomly distributed pores. The bounding box color shows the prediction of the simplified model for the fate of network: homogenization (blue) or channelization (red). The solid black line shows the transition boundary between channelization instability and homogenization.

So far we mainly focused on erosion dynamics with $m = 1$ (see Eq. (1)) since it directly corresponds to different physics of erosion in a network, i.e. an erosion rate with a linear dependence to fluid-flux, velocity, or shear-rate at the walls. Considering $m = 2$ in Eq. (1), our model aligns with the transport optimization problem in biological networks^{42,43,45}. Previous works have suggested that in the context of biological transport networks, the network is optimized to minimize its dissipation energy with regards to some constraint (such as constant material or metabolic cost). Interestingly, gradient descent utilized to find the minimal energy configurations maps to Eq. (1) with $m = 2$, albeit with additional regularizing terms. While under the dynamics we study here erosion will occur indefinitely, in biological transport networks a minimal energy configuration exists due to the additional constraints considered in their model. Nonetheless, the minimal energy configurations studied in these biological networks works manifest a phase transition reminiscent of the one we observe in our model. It would be interesting to see if the physical dynamics we have studied here can be mapped to gradient descent on an energy landscape for a general value of m . To show the effects of a general m in our model, we simulate the general form of erosion dynamics (Eq. (1)). The simulation results for a randomly initialized network for

method

Figure somehow
incorrectly placed.

they
pore
edge
is
identical

different powers of m and n is shown in Fig. 4, where each box shows the final snapshot of the network eroded with the corresponding m and n . We further compare the network's simulation result with the prediction of our simplified model for the fate of the network for each pair of m, n . The simplified model's prediction is shown using the bounding box color (red for channelization and green for homogenization) in Fig. 4. Additionally, the solid black line in Fig. 4 shows the simplified model's prediction for the boundary between network's transition to homogeneity or channelization. Although the simplified model is based on the erosion dynamics of two edges in a parallel or series configuration, it still correctly predicts the fate of the network with the complex topology for different values of m and n , and captures the boundary separating channelization/homogenization. We would like to point out that in the case of clogging, the initial dynamics can be captured using our model similarly, however at large times, due to the change in the connectivity

short!

of the network, our simplified model not extend to large time behaviors (see supplementary material S5).

Conclusion— In summary, we analyzed the dynamics of porous networks during erosion. We showed that depending on different erosion laws various network behaviors are observable. Using a simple erosion law, inspired by previously proposed models, we showed that depending on the rate of erosion the network can either move toward homogenization or toward developing a channeling instability. With a simplified model, we elucidated the physical origin of the phase transition. Our results signify the importance of local dynamics and feedback mechanism in long-time global behavior and complement similar feedback-induced studies for active conducting mediums⁴⁶.

Acknowledgments— We would like to thank Kavli Foundation, MRSEC DMR-2011754, and DMR-1420570 for their support.

-
- * A.Z. and D.P. contributed equally.
 † arielamir@seas.harvard.edu
- ¹ D. Fragedakis, C. Kouris, Y. Dimakopoulos, and J. Tsamopoulos, *Physics of Fluids* **27**, 082102 (2015).
 - ² M. Sahimi, *Flow and transport in porous media and fractured rock: from classical methods to modern approaches* (John Wiley & Sons, 2011).
 - ³ W. H. Schlesinger, *Science* **284**, 2095 (1999).
 - ⁴ J. Herzig, D. Leclerc, and P. L. Goff, *Industrial & Engineering Chemistry* **62**, 8 (1970).
 - ⁵ C. Tien and A. C. Payatakes, *AIChE Journal* **25**, 737 (1979).
 - ⁶ D. P. Jaisi, N. B. Saleh, R. E. Blake, and M. Elimelech, *Environmental Science & Technology* **42**, 8317 (2008).
 - ⁷ M. Carrel, V. L. Morales, M. A. Beltran, N. Derlon, R. Kaufmann, E. Morgenroth, and M. Holzner, *Water Research* **134**, 280 (2018).
 - ⁸ J. D. Seymour, J. P. Gage, S. L. Codd, and R. Gerlach, *Physical Review Letters* **93**, 198103 (2004).
 - ⁹ M. Duduta, B. Ho, V. C. Wood, P. Limthongkul, V. E. Brunini, W. C. Carter, and Y.-M. Chiang, *Advanced Energy Materials* **1**, 511 (2011).
 - ¹⁰ H. Sun, J. Zhu, D. Baumann, L. Peng, Y. Xu, I. Shakir, Y. Huang, and X. Duan, *Nature Reviews Materials* **4**, 45 (2019).
 - ¹¹ S. Marbach, K. Alim, N. Andrew, A. Pringle, and M. P. Brenner, *Physical Review Letters* **117**, 178103 (2016).
 - ¹² A. Tero, S. Takagi, T. Saigusa, K. Ito, D. P. Bebbert, M. D. Fricker, K. Yumiki, R. Kobayashi, and T. Nakagaki, *Science* **327**, 439 (2010).
 - ¹³ K. Alim, G. Amselem, F. Peaudecerf, M. P. Brenner, and A. Pringle, *Proceedings of the National Academy of Sciences* **110**, 13306 (2013).
 - ¹⁴ L. L. Heaton, E. López, P. K. Maini, M. D. Fricker, and N. S. Jones, *Proceedings of the Royal Society B: Biological Sciences* **277**, 3265 (2010).
 - ¹⁵ M. N. Rad, N. Shokri, and M. Sahimi, *Physical Review E* **88**, 032404 (2013).
 - ¹⁶ L. W. Lake, R. Johns, B. Rossen, G. A. Pope, *et al.*, *Fundamentals of Enhanced Oil Recovery*, (2014).
 - ¹⁷ S. Parsa, E. Santanach-Carreras, L. Xiao, and D. A. Weitz, *Physical Review Fluids* **5**, 022001 (2020).
 - ¹⁸ N. Schorghofer, B. Jensen, A. Kudrolli, and D. H. Rothman, *Journal of Fluid Mechanics* **503**, 357 (2004).
 - ¹⁹ A. Mahadevan, A. Orpe, A. Kudrolli, and L. Mahadevan, *Europhysics Letters* **98**, 58003 (2012).
 - ²⁰ R. Jäger, M. Mendoza, and H. J. Herrmann, *Physical Review E* **95**, 013110 (2017).
 - ²¹ L. Ristroph, M. N. Moore, S. Childress, M. J. Shelley, and J. Zhang, *Proceedings of the National Academy of Sciences* **109**, 19606 (2012).
 - ²² W. Hacking, E. VanBavel, and J. Spaan, *American Journal of Physiology-Heart and Circulatory Physiology* **270**, H364 (1996).
 - ²³ C. F. Wan and R. Fell, *Journal of Geotechnical and Geoenvironmental Engineering* **130**, 373 (2004).
 - ²⁴ H. Steeb, S. Diebel, and I. Vardoulakis, “Modeling internal erosion in porous media,” in *Computer Applications In Geotechnical Engineering*, pp. 1–10.
 - ²⁵ D. Marot, V. D. Le, J. Garnier, L. Thorel, and P. Audrain, *European Journal of Environmental and Civil Engineering* **16**, 1 (2012).
 - ²⁶ L. Sible, F. Lominé, P. Poullain, Y. Sail, and D. Marot, *Hydrological Processes* **29**, 2149 (2015).
 - ²⁷ N. J. Derr, D. C. Fronk, C. A. Weber, A. Mahadevan, C. H. Rycroft, and L. Mahadevan, *Physical Review Letters* **125**, 158002 (2020).
 - ²⁸ H. Yang and M. T. Balhoff, *AIChE Journal* **63**, 3118 (2017).
 - ²⁹ L. N. Reddi, X. Ming, M. G. Hajra, and I. M. Lee, *Journal of Geotechnical and Geoenvironmental Engineering* **126**, 236 (2000).
 - ³⁰ G. Boccardo, D. L. Marchisio, and R. Sethi, *Journal of Colloid and Interface Science* **417**, 227 (2014).
 - ³¹ K. Alim, S. Parsa, D. A. Weitz, and M. P. Brenner, *Physical Review Letters* **119**, 144501 (2017).
 - ³² I. Fatt *et al.*, *Transactions of the AIME* **207**, 144 (1956).
 - ³³ M. J. Blunt, B. Bijeljic, H. Dong, O. Gharbi, S. Iglauber,

- P. Mostaghimi, A. Paluszny, and C. Pentland, *Advances in Water resources* **51**, 197 (2013).
- ³⁴ N. Stoop, N. Waisbord, V. Kantsler, V. Heinonen, J. S. Guasto, and J. Dunkel, *Journal of Non-Newtonian Fluid Mechanics* **268**, 66 (2019).
- ³⁵ S. L. Bryant, P. R. King, and D. W. Mellor, *Transport in porous media* **11**, 53 (1993).
- ³⁶ S. Parsa, A. Zareei, E. Santanach-Carreras, E. Morris, A. Amir, L. Xiao, and D. A. Weitz, submitted (2021).
- ³⁷ D. Fragedakis, E. Chaparian, and O. Tammisola, *Journal of Fluid Mechanics* **911**, A58 (2021).
- ³⁸ L. T. Akanji and S. K. Matthai, *Transport in Porous Media* **81**, 241 (2010).
- ³⁹ S. S. Datta, H. Chiang, T. Ramakrishnan, and D. A. Weitz, *Physical Review Letters* **111**, 064501 (2013).
- ⁴⁰ C.-h. Liu, S. R. Nagel, D. Schecter, S. Coppersmith, S. Majumdar, O. Narayan, and T. Witten, *Science* **269**, 513 (1995).
- ⁴¹ S. Coppersmith, C.-h. Liu, S. Majumdar, O. Narayan, and T. Witten, *Physical Review E* **53**, 4673 (1996).
- ⁴² D. Hu and D. Cai, *Physical Review Letters* **111**, 138701 (2013).
- ⁴³ H. Ronellenfitsch and E. Katifori, *Physical Review Letters* **117**, 138301 (2016).
- ⁴⁴ B. Kramer and A. MacKinnon, *Reports on Progress in Physics* **56**, 1469 (1993).
- ⁴⁵ F. Corson, *Physical Review Letters* **104**, 048703 (2010).
- ⁴⁶ S. A. Ocko and L. Mahadevan, *Physical Review Letters* **114**, 134501 (2015).

Temporal Evolution in the Networks of Porous Materials: From Homogenization to Instability

Ahmad Zareei, Pan Deng, and Ariel Amir*

School of Engineering and Applied Sciences, Harvard University, Cambridge, MA, 02148

(Dated: May 20, 2021)

Also weak disorder, no!]

S1. SIMULATION ALGORITHM

In our simulations, we tested two types of network: a (i) diamond-grid network, and a (ii) topologically random network. In the diamond-grid network, we choose $N_x = 200$ edges in the horizontal direction and $N_y = 100$ edges in the vertical direction. The random network is created using uniformly distributed points with on average $N_x \times N_y$ edges in the horizontal and vertical directions. Note that the randomly distributed points are connected using a Delaunay triangulation. The diameter of each edge is sampled from either a uniform distribution in $r \in [1, 14]$, log-normal distribution with $\mu = 3, \sigma = 0.48$, or truncated normal distribution with $\mathcal{N}(\mu = 7.0, \sigma = 3.6)$. The external flow pressure is applied horizontally from left to right. An external pressure is then considered between the left-most nodes and the rightmost nodes ($p_{\text{left}} = 10, p_{\text{right}} = 0$). Assuming a Poiseuille flow in each edge, the fluid flow q and pressure difference δP_e in each edge is related through $q_e = C_e \delta P_e$, where $C_e = \pi r_e^4 / 8\mu L_e$, L_e is the length of the tube, and μ is the viscosity of the fluid. Let Δ be the transpose of the network's oriented incidence matrix. Note that the orientation of each edge is arbitrary since it only determines the positive direction of flow in that edge. Define $|q_e\rangle$ as the vector of flow through all the edges, then we have $|q_e\rangle = C_e \Delta |P_n\rangle$ where $|P_n\rangle$ is the vector of pressure at all the nodes. With a given boundary condition, we solve the equation through a modified nodal analysis as follows. The conservation of mass at each node can be written as

$$|q_n\rangle = \Delta^\top \mathbf{C} \Delta |P_n\rangle, \quad (\text{S1})$$

where $\mathbf{C} = \text{diag}(C_e^{(1)}, C_e^{(2)}, \dots, C_e^{(N_e)})$ is a diagonal matrix of edge conductances, and $|q_n\rangle$ is the vector of total incoming flow to each node. Note that total incoming flow to an internal node is zero inside the network due to the conservation of mass, and is only non-zero at the boundary nodes. Renumbering the boundary nodes to $1, 2, \dots, N_B$, we can partition Eq. (S1) to obtain

$$\begin{bmatrix} \Delta_b^\top \mathbf{C} \Delta_b & \Delta_b^\top \mathbf{C} \Delta_n \\ \Delta_n^\top \mathbf{C} \Delta_b & \Delta_n^\top \mathbf{C} \Delta_n \end{bmatrix} \begin{bmatrix} P_1^{BC} \\ P_2^{BC} \\ \vdots \\ P_{N_B}^{BC} \\ \hline P_{N_B+1} \\ \vdots \\ P_{N_n} \end{bmatrix} = \begin{bmatrix} q_1^{BC} \\ q_2^{BC} \\ \vdots \\ q_{N_B}^{BC} \\ 0 \\ \vdots \\ 0 \end{bmatrix} \rightarrow \begin{bmatrix} \mathbf{A}_{bb} & \mathbf{A}_{bn} \\ \mathbf{A}_{nb} & \mathbf{A}_{nn} \end{bmatrix} \begin{bmatrix} P_1^{BC} \\ P_2^{BC} \\ \vdots \\ P_{N_B}^{BC} \\ \hline P_{N_B+1} \\ \vdots \\ P_{N_n} \end{bmatrix} = \begin{bmatrix} q_1^{BC} \\ q_2^{BC} \\ \vdots \\ q_{N_B}^{BC} \\ 0 \\ \vdots \\ 0 \end{bmatrix}, \quad (\text{S2})$$

where $\mathbf{A}_{st} = \Delta_s^\top \mathbf{C} \Delta_t^\top$ and $s, t \in \{a, b\}$. In summary the above equations simplifies to

$$\begin{cases} \mathbf{A}_{bb} |P_{BC}\rangle + \mathbf{A}_{bn} |P\rangle = |q_{BC}\rangle, \\ \mathbf{A}_{nb} |P_{BC}\rangle + \mathbf{A}_{nn} |P\rangle = 0. \end{cases} \quad (\text{S3})$$

Solving the above equations results in the nodes' pressure and also the fluid flux at the boundary nodes. With the flux at each edge, q_e , the increase (decrease) of tube radius under erosion (clogging) is obtained as

$$\frac{dr_e}{dt} \propto \pm \frac{q_e}{r_e^n}. \quad (\text{S4})$$

* arielamir@seas.harvard.edu

Supply code in github?

We use simple forward Euler for time integration. For each iteration, we choose the time step dt so that $\max(dr_e) = 0.1r_0$, where r_0 is the smallest radius among all edges. Note that $r_{ij}(t + \delta t) = r_{ij}(t) + (\alpha\delta t)q_{ij}(t)/r_{ij}^n(t)$, where the coefficient $\alpha\delta t$ is chosen such that the maximum change in the radius at each time step is smaller than one-tenth of the smallest tube's radius i.e. $\max(\Delta r_{ij}) \leq r_{\min}/10$ of the smallest radius at the initial configuration. This condition guarantees that at each step a small amount of material is eroded and there's no sudden change in the network. We further test the convergence by decreasing $\max(\Delta r_{ij})$ to half and we observe that the average relative change in the flux vector becomes 1.2%, and the PDFs remain intact without any change.

IS

notable

repetitive.

mention we are repeating a known derivation.

S2. ANALYTICAL RESULTS

As described in the main text, the PDF of flow in a topologically disordered network of tubes is the same as a structured diamond grid when the radius of the tubes is highly disordered. In this section, we show that the observed exponential distribution of fluid flux can be described using a mean-field approach on a structured grid. Basically, the random distribution of the diameters along with the conservation of mass in the network are the two main ingredients resulting in an exponential tail distribution. In a diamond grid, the incoming flow to a node is redistributed among the outgoing edges (since fluid mass is conserved). Due to the randomness in the tube's diameter, one can imagine that the redistribution of the incoming flow to a node between the outgoing edges is random variable. The only condition required to hold here is that the incoming flux should be equal to the outgoing flux. This model for the flow can be mapped one to one to the problem of force fluctuations in a bead pack [1–3] as shown in Fig. S1. In a bead pack, the force at each layer is redistributed to the next layer where the total force exerted on the next layer should equal to that of the previous layer. Given the above conditions, the flow at layer $L + 1$ at node j can be obtained as

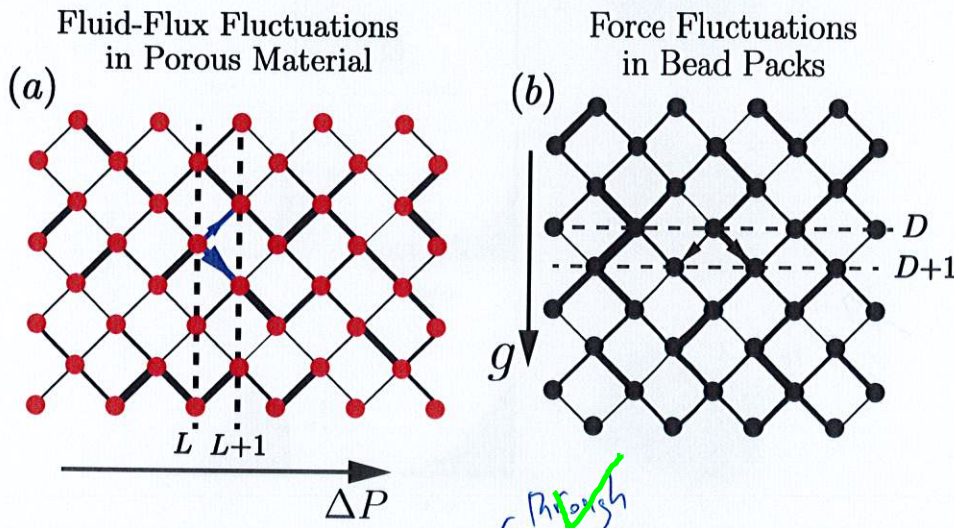


FIG. S1. (a) Schematic of diamond grid network of tubes. The incoming flow to each node is redistributed among the outgoing edges. The thickness of the lines shows the fluid flux transferred in that edge. (b) Schematic diagram showing beads (represented with nodes) and their contacts to the neighboring sites (represented with edges). The thickness of the edges show the weight transferred through that contact.

$$q(L+1, j) = \sum_i w_{ij} q(L, i) = w_{i,i+1} q(L, i+1) + w_{i,i} q(L, i), \quad (S5)$$

where w_{ij} shows the weights by which the flow is redistributed. Note that since the total fluid flux is conserved, then $\sum_j w_{ij} = 1$. Assuming a general distribution of $\eta(w)$, we can use the mean-field approximation to find the distribution of q at the layer L , i.e., $p_L(q)$. The values of $q(L, i)$ are not independent for neighboring sites; however, in our mean-field approximation we ignore such correlations. We find

$$p_L(q) = \prod_{j=1}^N \left\{ \int_0^1 dw_j \eta(w_j) \int_0^\infty dq_j p_{L-1}(q_j) \right\} \times \delta \left(\sum_j w_j q_j - q \right), \quad (S6)$$

where N is the number of outgoing edges (e.g., in our structured diamond grid $N = 2$) and $\delta(\cdot)$ is the Kronecker delta function. Note that the constraint that q 's emanating downward should add up to one is in the definition of $\eta(w)$. Taking the Laplace transform of the above equation and defining $\tilde{p}(s) \equiv \int_0^\infty p(q) e^{-qs} dq$ we obtain

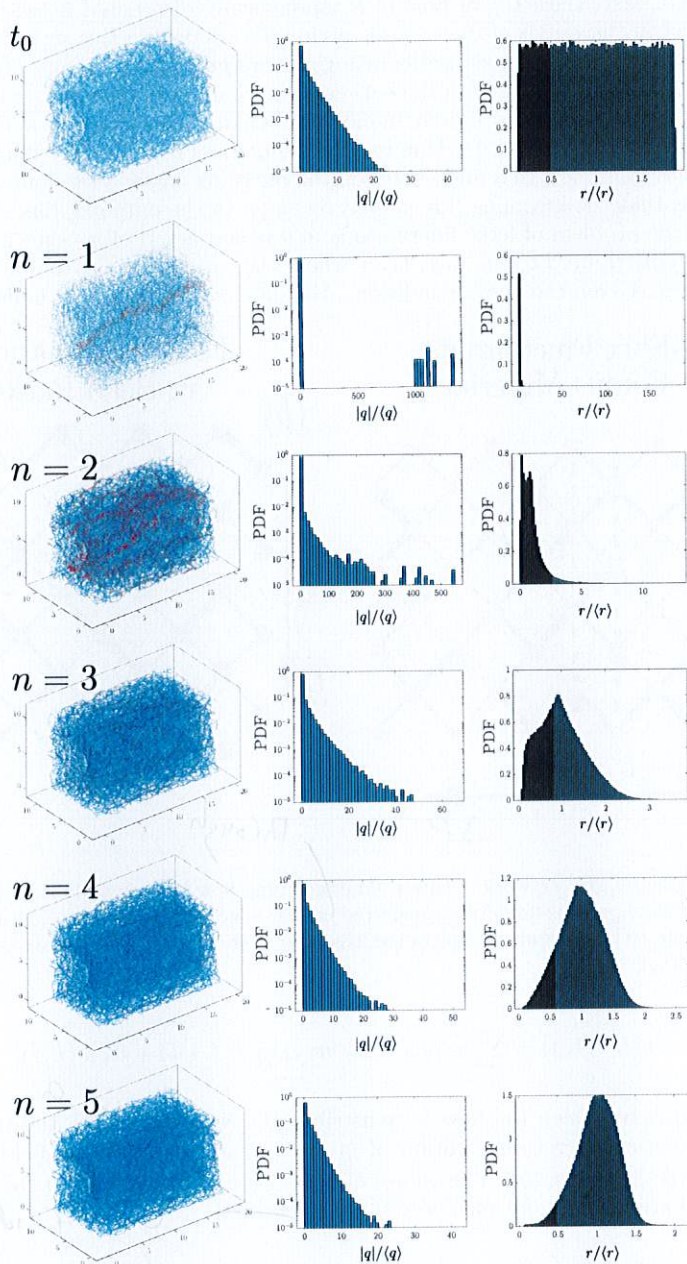
$$\tilde{p}_L(s) = \left(\int_0^1 dw \eta(w) \tilde{p}_{L-1}(sw) \right)^N. \quad (S7)$$

The probability distribution at the layers converges to a distribution $\tilde{p}(s)$. The final solution for a structured diamond grid with two neighboring sites becomes $p(q) = 4q \exp(-2q)$ [1–3], which is a distribution with an exponential tail.

[we → one to emphasize this is not original]

S3. ADDITIONAL NUMERICAL RESULTS

Nice a few
lines of text...
parameters
etc.



Made
larger?

FIG. S2. Erosion in a topologically random 3D network of tubes with an initial broad distribution of tube diameters. The first row shows the initial condition at $t = 0$. Each row afterward corresponds to the simulation result after N steps such that $\langle r_{t=N} \rangle = 2r_0$ where $r_0 = \langle r_{t=0} \rangle$. The erosion law is based on Eq. (1) in the main text where different powers of n correspond to different models of erosion. The first column is a snapshot of the pore network, the second column is the PDF of normalized fluid flux $q/\langle q \rangle$, and the last column is the PDF of normalized radius $r/\langle r \rangle$.

S4. AVERAGE CHANGE IN THE ORDER PARAMETER

???

Does this correspond to Fig. S5?

S5. CLOGGING DYNAMICS

Besides erosion, another change in the network is the deposition/sedimentation of material on the boundary walls of the porous material. We name this dynamical change a “clogging” process as opposed to erosion. Contrary to erosion, the clogging behavior may cause some edges to block which effectively alters the network of connectivity and network behavior. This change in the connection between nodes through edges getting blocked can drastically alter porous structure behavior, e.g., causes a huge difference between effective and true porosity [4]. Despite the drastic change of network with blockages, we can still focus on the *initial* change in the order parameter. The derivative of order parameter can be written as

$$\frac{d\mathcal{O}}{dt} = \sum_{ij} \sum_{kl} \frac{\partial \mathcal{O}}{\partial q_{ij}} \frac{\partial q_{ij}}{\partial C_{kl}} \frac{\partial C_{kl}}{\partial t} \quad (\text{S8})$$

where the last term changes sign from erosion to clogging, i.e., $\partial C_{kl}/\partial t = \pm \alpha \pi q_{kl}/r_{kl}^{n-3} \mu l_{kl}$ for erosion and clogging respectively. As a result, the magnitude of change in the order parameter equals that of erosion. Note that in Eq. (S8), the second term depends on the network topology, and pore throat clogging results in the change of network topology at later times. At short times, however, similar to the erosion, a phase transition exists at $n = 3$. When $n < 3$ the network moves toward homogenization during the clogging process and when $n > 3$ the flow moves toward the development of channeling instability. At later times, this initial trend, however, might not hold true due to the aforementioned complex changes in the connectivity network during the clogging process.

-
- [1] C.-h. Liu, S. R. Nagel, D. Schecter, S. Coppersmith, S. Majumdar, O. Narayan, and T. Witten, Force fluctuations in bead packs, *Science* **269**, 513 (1995).
 - [2] S. Coppersmith, C.-h. Liu, S. Majumdar, O. Narayan, and T. Witten, Model for force fluctuations in bead packs, *Physical Review E* **53**, 4673 (1996).
 - [3] K. Alim, S. Parsa, D. A. Weitz, and M. P. Brenner, Local pore size correlations determine flow distributions in porous media, *Physical Review Letters* **119**, 144501 (2017).
 - [4] S. Parsa, A. Zareei, E. Santanach-Carreras, E. Morris, A. Amir, L. Xiao, and D. A. Weitz, Unexpected scaling of interstitial velocities with permeability due to polymer retention in porous media, *arXiv* (2021).

*Pristine
communication*

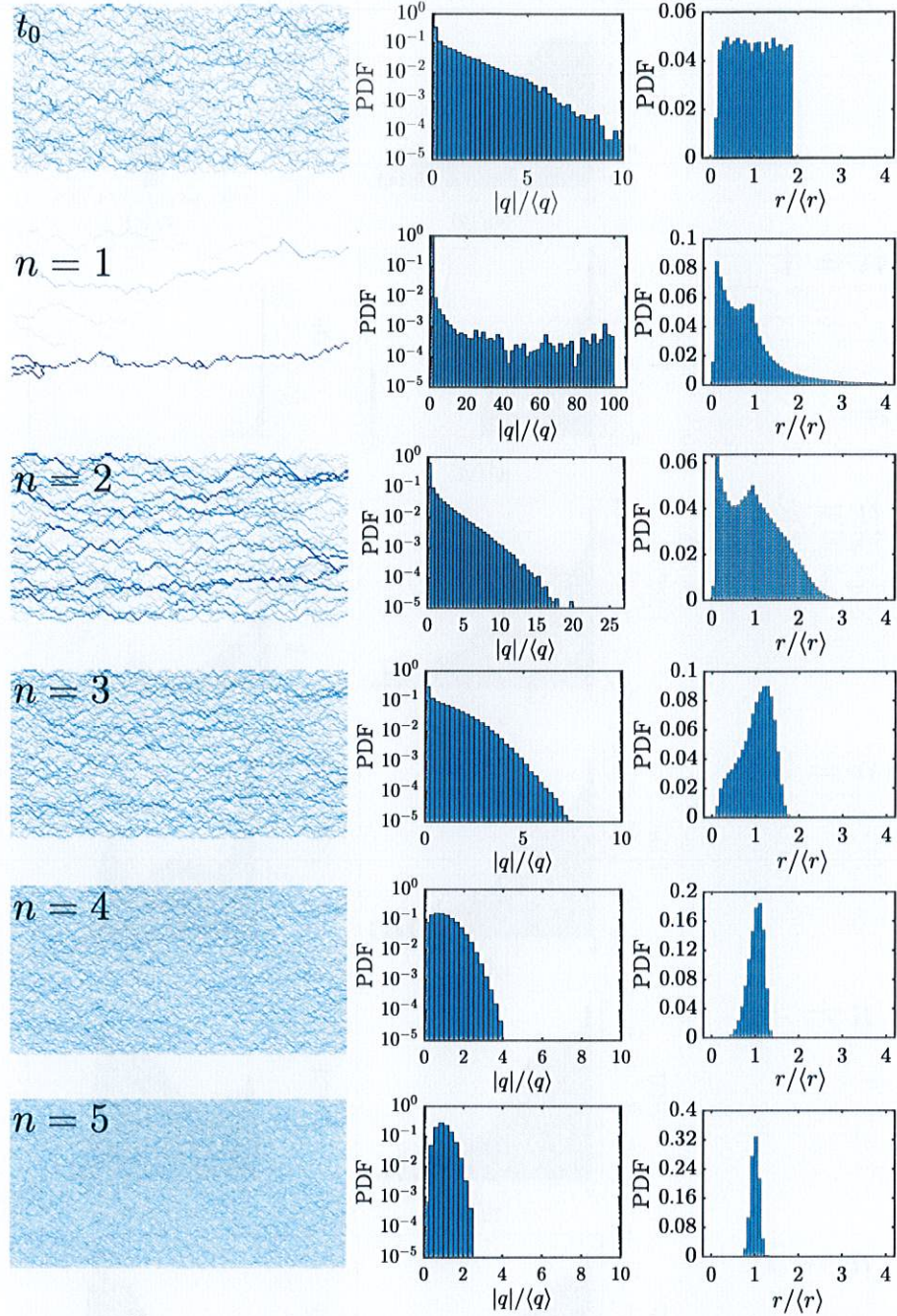


FIG. S3. Erosion in a diamond grid of networks with an initially broad distribution of tube diameter. The initial condition is shown with the label $t = 0$ in the first row. Each row afterward corresponds to the simulation result after N steps such that $\langle r_{t=N} \rangle = 2r_0$ where $r_0 = \langle r_{t=0} \rangle$ or twice the initial average radius. The erosion law is based on Eq. (1) in the main text where different powers of n correspond to different models of erosion. The first column is a snapshot of the pore network, the second column is the PDF of normalized fluid flux $q/\langle q \rangle$, and the last column is the PDF of normalized radius $r/\langle r \rangle$.

Put into section
rather than "floating"
have
(same for S4, S5)
e.g. Section 07
"Robustness of results"

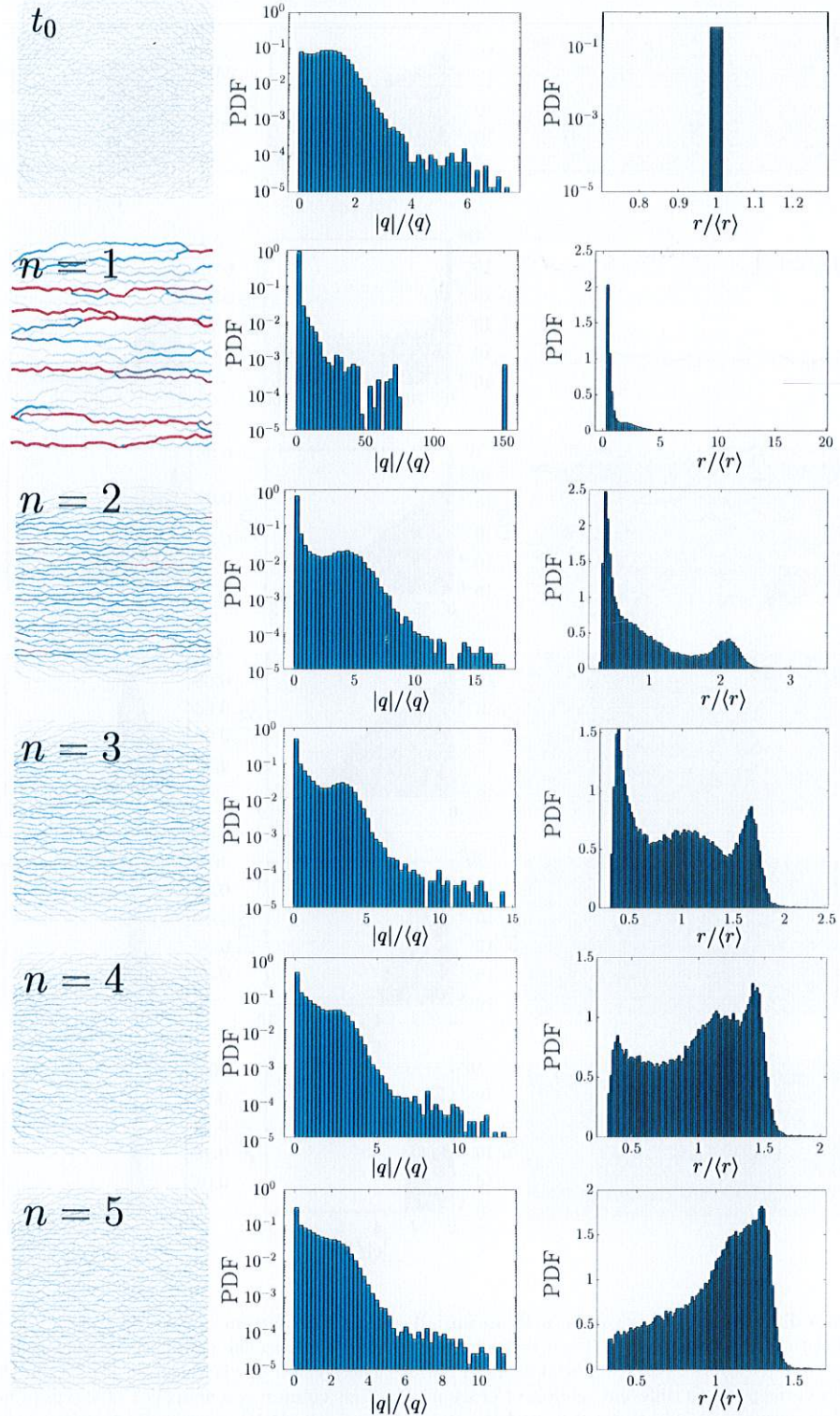


FIG. S4. Erosion in a random network of tubes with an initially narrow distribution of tube diameters of $d_0(1 + \epsilon)$ where ϵ is a uniform random number in $[-0.03, 0.03]$. The initial condition is shown with the label $t = 0$ in the first row. Each row afterward corresponds to the simulation result after N steps such that $\langle r_{t=N} \rangle = 2r_0$ where $r_0 = \langle r_{t=0} \rangle$ or twice the initial average radius. The erosion law is based on Eq. (1) in the main text where different powers of n correspond to different models of erosion. The first column is a snapshot of the pore network, the second column is the PDF of normalized fluid flux $q/\langle q \rangle$, and the last column is the PDF of normalized radius $r/\langle r \rangle$.

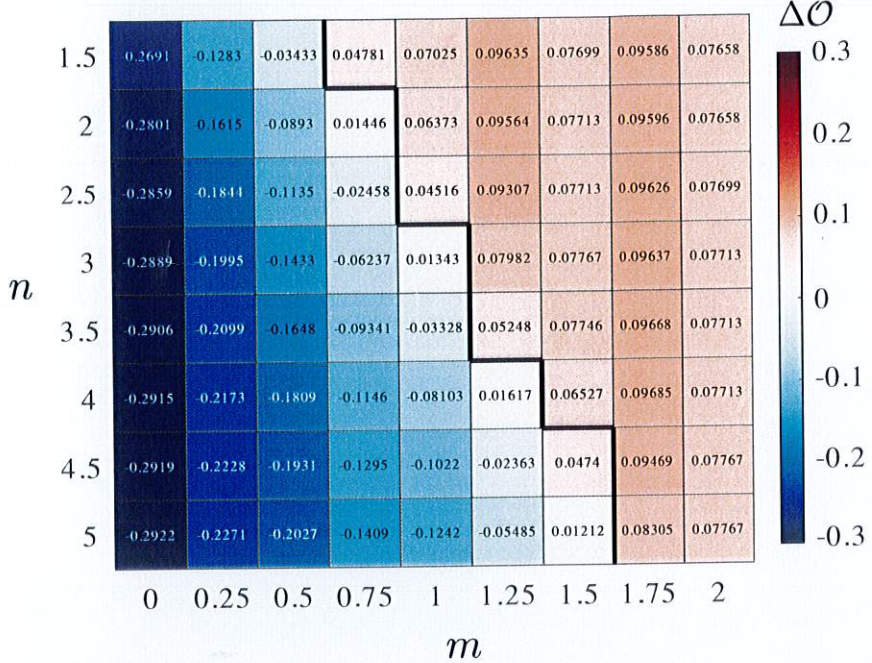


FIG. S5. The heat map for the average change in the order parameter for 100 simulations. Networks with $N_x = 50$ and $N_y = 50$ are randomly initialized (both network topology and edge diameters) and then the network is evolved using Eq. (1) of the main text for different n and m until $\langle r \rangle = 2r_0$ where r_0 is the initial average diameter distribution. The heatmap shows the change in the order parameter for such networks averaged over 100 different simulations. The black line shows the boundary between homogenization and channelization obtained using the simplified model.

